NASA TECHNICAL NOTE

NASA TN D-3141

NASA TN D-3141

DEPENDENCE OF ADSORPTION PROPERTIES ON SURFACE STRUCTURE FOR BODY-CENTERED-CUBIC SUBSTRATES

by Robert J. Bacigalupi and Harold E. Neustadter

Lewis Research Center
Cleveland, Ohio

NATIONAL AERONAUTICS AND SPACE ADMINISTRATION • WASHINGTON, D. C. • DECEMBER 1965

NASA TN D-3141

DEPENDENCE OF ADSORPTION PROPERTIES ON SURFACE STRUCTURE FOR BODY-CENTERED-CUBIC SUBSTRATES

By Robert J. Bacigalupi and Harold E. Neustadter

Lewis Research Center
Cleveland, Ohio

NATIONAL AERONAUTICS AND SPACE ADMINISTRATION

For sale by the Clearinghouse for Federal Scientific and Technical Information
Springfield, Virginia 22151 – Price $1.00

DEPENDENCE OF ADSORPTION PROPERTIES ON SURFACE STRUCTURE FOR BODY-CENTERED-CUBIC SUBSTRATES

by Robert J. Bacigalupi and Harold E. Neustadter

Lewis Research Center

SUMMARY

The Lennard-Jones 6-12 atom interaction potential is applied to the calculation of adsorption energy of an atom onto as many as 132 sites on a unit cell area of each of the eight highest surface density planes of a body-centered-cubic substrate. From the calculations, topographical maps of adsorption energy on a unit cell area of each plane for various adsorbate-adsorbent combinations are plotted. Normalized values of maximum adsorption energies and minimum surface diffusion activation energies for all cases are tabulated. The results are compared with available experimental data concerning adsorption of alkali metals, alkali earth metals, and inert gases on transition metal substrates and are in good agreement. Application of the results to transition-metal - transition-metal combination predicts that the 110 surface is the lowest energy configuration for a body-centered-cubic crystal.

INTRODUCTION

Adsorption on an atomic scale gained recognition with the advent of the field-ion microscope and field-emission microscope, and it gained in importance proportionally with the fields of ultrahigh vacuum, gas-filled thermionic converters and the contact-ionization engine. Through the use of field-ion and field-emission microscopy, it has been observed that adsorption properties are strongly dependent on the atomic arrangement of the substrate (in some cases more so than on the materials involved). Forces governing adsorption of many species on metals or semiconductors have been found to be of the form of dispersion forces such as van der Waal forces (ref. 1). By considering dispersion force interactions of an adsorbing atom with the nearest neighbors of the substrate, one can verify that the substrate structure grossly affects the adsorption properties (refs. 2 and 3). It is the intent of this report to calculate the interaction potential encountered by a single atom at any point on various ideal single crystal planes of the body-centered-cubic structure. Furthermore, it is intended to deduce from such potential surfaces some general properties of physical adsorption and specific properties, such as adsorption energy and diffusion activation energy, and to compare these results with experimental observations.

→ 2

The Lennard-Jones 6-12 potential is used as a model. Its applicability to adsorption of a nonpolar[1] atom on a metal is discussed in the following section. The general mathematical techniques employed are outlined in the section PROCEDURE, while details concerning the performance of the specific lattice summations for the body-centered-cubic structure are contained in appendix A. The last section compares the results with the scant experimental data and discusses the application of the results to known adsorption characteristics of practical surfaces.

→ P. 6

MODEL

The Lennard-Jones potential is (ref. 2)

$$E = 4\epsilon\left[-\left(\frac{\sigma}{r}\right)^6 + \left(\frac{\sigma}{r}\right)^{12}\right] \tag{1}$$

where E is the atom-atom interaction energy, ϵ is the depth of the energy well, σ is that finite value of r for which E is zero, and r is the internuclear distance. The attractive portion of equation (1) is proportional to the inverse sixth power and represents a long-range van der Waals interaction, while the repulsive contribution is approximated by an inverse twelfth power dependence.

Application of this atom-atom interaction potential to adsorption on a solid assumes additivity of the interaction of the adsorbate with each atom of the adsorbent or

$$\varphi = 4\epsilon\sum_i\left[-\left(\frac{\sigma}{r_i}\right)^6 + \left(\frac{\sigma}{r_i}\right)^{12}\right] \tag{2}$$

where φ is the atom-metal interaction energy and r_i is the distance from the adsorbed atom the i^{th} atom of the substrate. Thus, effects arising specifically from the structure of the substrate are contained in the lattice summations, $\sum_i r_i^{-6}$ and $\sum_i r_i^{-12}$ whereas effects arising from the atomic properties of the constituent atoms are contained in the parameters σ and ϵ. Appendix B contains a discussion of the physical meanings of both σ and ϵ.

Equation (2) neglects any contribution to the interaction by free electrons in the solid; however, a study by Pierotti and Halsey (ref. 4) on the interaction of krypton atoms with metals has shown that theories which include the free electron contribution of the metal do not give significantly improved results as opposed to theories in which the free electron contributions are ne-

[1]All atoms have instantaneous dipole moments that are the primary source for the long range interactions between atoms. An atom is considered nonpolar if when isolated its net dipole moment is zero over a period of time.

glected. Neustadter, Luke, and Sheahan (ref. 5) have further shown that very low coverage adsorption of various alkali metal atoms on tungsten can be satisfactorily explained by using equation (2). Of course, the validity of the proposed model can best be tested by comparing the calculated results with experimental data.

PROCEDURE

In order to preserve the general applicability of this work to adsorption on any substrate, equation (2) is rewritten as

$$\frac{\varphi}{4\epsilon} = \left[\left(\frac{\sigma}{a_o}\right)^{12} \sum_i \left(\frac{1}{d_i}\right)^{12} - \left(\frac{\sigma}{a_o}\right)^{6} \sum_i \left(\frac{1}{d_i}\right)^{6}\right] \tag{3}$$

where d_i is r_i/a_o, and a_o is the lattice constant of the substrate. Equation (3) is treated as follows: For each surface orientation considered, a coordinate system is chosen such that the x,y plane passes through the centers of all the surface atoms and z is positive along the outward normal. Clearly $\varphi/4\epsilon$ is a function of x, y, and z.

As shown in sketch (c) of appendix A (p. 9) each unit cell is broken up into a grid of as many as 132 prospective adsorption sites where the number of sites is chosen so that each unit cell will have approximately the same density of prospective sites. At any one of these sites (x_j,y_j) the sums $\sum_i d_i^{-6}$ and $\sum_i d_i^{-12}$ are evaluated as functions of z. Using these sums in equations (3) and plotting $\varphi/4\epsilon$ as a function of z yield, for example, sketch (a) (which will depend on surface orientation, site, and σ/a_o for its specific form).

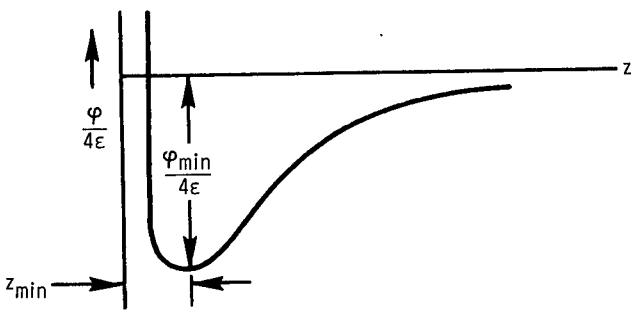

(a)

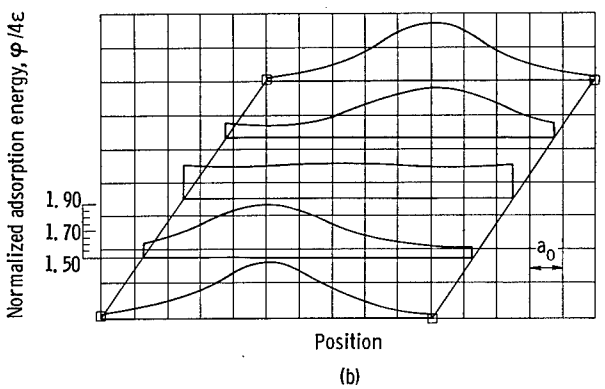

(b)

The assertion is made that, if adsorption were to occur over site x_j,y_j, the nucleus of the particle would be located at z_{min}, and the bond energy would be $\varphi_{min}/4\epsilon$ (where the quantities are as defined in sketch (a)). The derivative of $\varphi/4\epsilon$ is taken (numerically) with respect to z, and $\varphi_{min}/4\epsilon$ and z_{min} are calculated for a specific σ/a_o (see appendix A). This entire process is now repeated for each predetermined location x_j,y_j on a unit cell of the adsorbent. Then $\varphi_{min}/4\epsilon$ is

plotted as a function of surface coordinates x and y. An example of such a plot is shown in sketch (b) for the 110 plane and $\sigma/a_o = 1.00$ (corresponding to barium on tungsten). Here one unit cell of surface area is represented with the locations indicated for the substrate atoms nearest the surface. Along each of five equally spaced lines of constant y, $\varphi_{min}/4\epsilon$ is plotted against x with the ordinate $\varphi_{min}/4\epsilon$ in the y-direction.

The minimum value of $\varphi_{min}/4\epsilon$ is read graphically and is listed in table I. These values are the normalized heat of adsorption $\Phi/4\epsilon$ for the preferred adsorption site, for a specific orientation, and for a specific value of σ/a_o. The quantity $E_d/4\epsilon$ is also determined graphically by identifying it with the least amount of energy that must be supplied to an adsorbed atom to enable it to move from one preferred adsorption site to another, where the assumed path was not necessarily a straight line. In the 110, 210, and 310 cases, the topographical potential plots were obtained by manually cross-plotting the data for $\varphi_{min}/4\epsilon$ against position. In the remaining cases, the topographical potential plots were generated directly by a Fourier interpolation 7090 program from the original digital output. This procedure was made possible by using the fact that the potential is periodic along any line parallel to a border of the unit surface cell. This entire procedure is repeated for a range of values of σ/a_o and the remaining substrate orientations. For the specific summation technique applied to the body-centered-cubic structure see appendix A.

DISCUSSION OF RESULTS

The minimum values of $\varphi/4\epsilon$ and $E_d/4\epsilon$ are listed in table I. The original plots of the potential variation, such as illustrated in sketch (b), were replotted as topographical maps showing lines of equal adsorption energy. The eight highest surface density planes were considered (110, 100, 211, 310, 111, 321, 411, and 210 in order of decreasing density) and are presented in figures 1 to 8, respectively. Included in the topographical maps are the locations of the substrate atoms in each unit cell. The most probable migration direction is assumed to be path of least resistance (minimum $E_d/4\epsilon$) connecting two equivalent adsorption sites.

The values of σ/a_o used in the calculations were 0.80, 0.894, 1.00, 1.123, and 1.20. Table II lists the values of σ/a_o corresponding to various adsorbent-adsorbate combinations. The most meaningful interpretation of these data results from considering the comparative effects of substrate surface structure (crystal orientation) on adsorption and diffusion for a given combination of adsorbent and adsorbate (i.e., for a given σ/a_o).

The Lennard-Jones potential model corresponds most closely to inert gas atoms adsorbing on a semiconductor or an insulator when the coverage is low enough to eliminate any interaction of adsorbate atoms with one another. This limit of coverage is shown experimentally in some cases to be as high as 0.7 (e.g., thorium, ref. 6), thus allowing the calculations to be useful in practical systems at coverages other than zero. The Lennard-Jones potential model has been used in calculating adsorption energies of various metals on

tungsten (ref. 7) and, in particular, adsorption energies of alkali metals on tungsten (ref. 5). Agreement of the results with experimental data implies that this method may also be applied to other metal-metal systems. Substrates that are compared are assumed to be atomically smooth ideal crystal planes with no dislocations, steps, impurities, missing atoms, or surface relaxations. The experimental situation most closely approaching these assumptions exists in the field-emission microscope in which the tip is an annealed single crystal with a minimum of imperfections and on which there are small areas of atomically smooth planes.

In emission-microscope experiments by Utsugi and Gomer (ref. 8) and Drechsler (ref. 9) who studied the adsorption of barium on tungsten, the activation energies for diffusion E_d on the 110 and 321 planes were measured and were in good agreement with the calculated results as follows:

Measured:

$$\frac{(110)E_d}{(321)E_d} = \frac{0.41}{0.83} = 0.49 \text{ (Ref. 8)} \qquad \frac{(110)E_d}{(321)E_d} = \frac{0.20}{0.65} = 0.31 \text{ (Ref. 9)}$$

Calculated:

$$\frac{(110)E_d/4\epsilon}{(321)E_d/4\epsilon} = \frac{0.135}{0.345} = 0.39$$

Experimental data such as these may be used to evaluate ϵ empirically, which in turn may be used to obtain quantitative values for E_d and Φ for each plane of a given system (i.e., given σ/a_o). An alternative theoretical expression for ϵ is presented in appendix B.

Calculated adsorption energies from table I (with $\sigma/a_o \cong 1.00$ for xenon on tungsten and molybdenum) agree favorably with emission microscope experiments by Ehrlich and Hudda (ref. 10), who studied the adsorption of xenon on tungsten and molybdenum. They found stability of the adsorbate highest on the 210, 310, and 611 planes, lower on the 211 plane, and lowest on the 100 and 110 planes at temperatures where diffusion is not important. This remarkable agreement is less surprising when one considers that the model is best suited to inert gas interactions.

Adsorption of cesium on transition metals is of considerable interest in those applications related to electron and ion emission. Unfortunately, the adsorption energy of cesium on various planes of metals is not as well documented as that of inert gases on metals. It has been repeatedly observed (e.g., see ref. 11) that the 110 plane of both molybdenum and tungsten has a higher current density than any other plane at a given substrate temperature and cesium arrival rate (in the region of low to intermediate coverages). Since this plane has the highest vacuum work function, these observations have been interpreted as implying a maximum stability of cesium on the 110 surface, whereas

the calculations predict that cesium should be least stable on the 110 plane of tungsten ($\sigma/a_o = 1.123$). However, one may attribute increased emission density from a partly covered plane to any one or combination of the following three factors:

(1) High stability of the adsorbate on the plane in question, which depends exponentially on Φ and E_d

(2) High number of sites available for adsorption

(3) Large effective dipole moment of an adsorbed particle

The 110 plane has the highest density of sites available of all body-centered-cubic planes. Good and Müller (ref. 6) have shown that for a given surface density of adatoms the 110 showed by far the greatest decrease in work function of all body-centered-cubic planes. The relatively large emission density from the 110 plane of tungsten partly covered with cesium is not sufficiently definitive of adsorption energies to provide an adequate test of the Lennard-Jones potential model.

In general, the calculations substantiate the prevalent model of surface adsorption in which discrete adsorption sites exist and in which diffusion is defined as the motion of atoms between well-defined sites. Also the calculations verify the expectation that these sites exist at wells in the surface where the outer electrons of adsorbate participate in binding with a maximum number of substrate atoms.

Additional verification of the validity of the calculations is realized in examining self-adsorption and self-diffusion. The lowest energy surface configuration of a body-centered-cubic crystal of tungsten (refs. 12 and 13) was shown experimentally to be the 110 surface, where the experimental situation closely approaches that assumed in the calculations. Recognizing the relatively low values of $\Phi/4\epsilon$ and $E_d/4\epsilon$ at $\sigma/a_o = 0.80$ ($\sigma/a_o = 0.786$ for self-adsorption) for the 110, 100, and 211 planes (in that order) one can see that the calculations predict that, for a body-centered-cubic crystal annealed in vacuum, the final surface would consist of 110 planes, while, in the transition, the 100 and 211 planes have a high probability of existing. It must be noted here that even though the physical mechanism of metallic binding may not be described exactly by the Lennard-Jones potential, the structure-dependent adsorption properties of such a system can be readily predicted by using the Lennard-Jones potential summation.

SUMMARY OF RESULTS

The following four factors serve to support the applicability of the results to practical adsorption phenomenon:

1. The general picture of adsorption, as observed experimentally, is verified because atomically rough surfaces tend to have higher heats of adsorption than closer packed surfaces.

2. More specifically, the order of heats of adsorption for xenon on various planes of tungsten is the same as that observed in field-emission-microscope experiments.

3. The equilibrium surface of body-centered cubic crystals is the 110 plane determined both by experiment and calculation.

4. The relative diffusion activation energy for barium on tungsten is in good agreement with measured values. The possible extension of these calculations to the adsorption properties of other structures (e.g., face-centered-cubic, diamond, etc.) and of single-crystal surfaces with various imperfections (e.g., missing atoms and steps) can readily be seen. end

Lewis Research Center,
National Aeronautics and Space Administration,
Cleveland, Ohio, August 6, 1965.

APPENDIX A

DETAILS OF THE SUMMATION FOR BODY-CENTERED-CUBIC SUBSTRATES

The location of all atoms in a body-centered-cubic crystal with respect to the coordinate system described previously has been recorded by Bacigalupi (ref. 14) for twenty orientations. This technique can be adapted to the present problem to define the four quantities $\bar{S}$, $\bar{X}$, $\bar{V}$, and d, where $\bar{S}$ locates the nearest surface atom to any surface atom, $\bar{X}$ locates the nearest surface neighbors in the x-direction to any surface atom, $\bar{V}$ connects any surface atom to the closest atom in the next-to-surface plane, and d is the interplanar distance measured along the z-axis. The vectors $\bar{X}$ and $\bar{S}$ form a unit cell of the surface as shown in sketch (c).

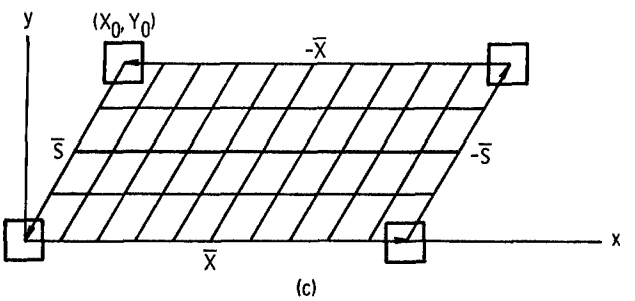

(c)

With these definitions and equation (A1) all the atoms in the crystal with respect to the surface plane can be located

$$\left.\begin{aligned} X_i &= X_o + I_i|\bar{V}(X)| + n|\bar{X}| + C \\ Y_i &= Y_o + I_i|\bar{V}(Y)| + m|\bar{S}(Y)| \\ C &= \left[Y_i - Y_o - I_i|\bar{V}(Y)|\right]\frac{|\bar{S}(X)|}{|\bar{S}(Y)|} \end{aligned}\right\} \qquad (A1)$$

where X_i, Y_i is the location of any atoms referred to the surface plane (x,y plane), X_o, Y_o is the starting point and location of the upper left corner of the unit cell, I_i is the plane in which the i^{th} atom exists (0 for surface plane; 1 for next-to-surface plane, etc.) (X) or (Y) indicates the component of the particular vector, and n and m are integers.

In performing the summations, it was necessary to establish a cutoff for the computer. Using an integral approximation to determine the contribution of those terms omitted from the summation leads to the result that accuracy to within 1 percent is achieved when the summation is extended over all the atoms within seven a_o of the site being considered. Therefore equation (A2) is introduced to establish the cutoff:

$$\left.\begin{aligned} X_o + 7.0 + |\bar{X}| > X_i > X_o - 7.0 \\ Y_o + 7.0 > Y_i > Y_o - 7.0 + |\bar{S}(Y)| \end{aligned}\right\} \qquad (A2)$$

The prospective adsorption sites for which the summations were performed are located at the intersections of five to ten equidistant lines parallel

to $\bar{X}$ and eleven to twenty equidistant lines parallel to $\bar{S}$, as shown in sketch (c). The distance r_i from an adsorbing atom to the i^{th} atom in the crystal can now be evaluated as a function of z. At each site, d_i (defined by eq. (A3))

$$d_i = \left[\left(X_i - X_o\right)^2 + \left(Y_i - Y_o\right)^2 + \left(I_i d + z\right)^2\right]^{1/2} \tag{A3}$$

was evaluated for each of sixty evenly spaced values of z ranging from 0.05 a_o to 2.1 a_o. The corresponding values of d_i were used in the summation in equation (3). The minimum value of $\varphi/4\epsilon$ obtained from equation (3) for a given site was used along with one value of $\varphi/4\epsilon$ in the negative z-direction and three values in the positive z-direction. A fourth-order equation was fitted to these five points, and a minimum was determined. The minimum was further corrected by using the Newton-Raphson method. Sketch (b) is an example of these minima plotted as a function of their position for the 110 plane for $\sigma/a_o = 1.00$.

APPENDIX B

EVALUATION OF σ/a_o AND ϵ

The Lennard-Jones potential (ref. 2) for interactions between two atoms is

$$E = 4\epsilon\left[-\left(\frac{\sigma}{r}\right)^6 + \left(\frac{\sigma}{r}\right)^{12}\right] \tag{1}$$

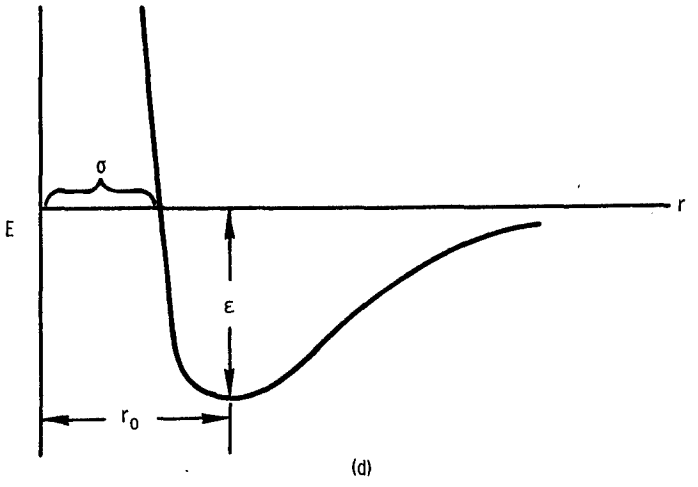

(d)

which graphically is of the form shown in sketch (d), where σ is that finite value of r for which $E = 0$, ϵ is the interaction bond energy of the two atoms, and r_o is their internuclear equilibrium distance.

To evaluate σ note that r_o is that value of r for which E is a minimum. Therefore, σ can be related to r_o by setting $(\partial E/\partial r)_{r_o} = 0$. This gives $\sigma = r_o 2^{-1/6}$. Since r can be approximated as the sum of the hard-sphere radii of the two interacting atoms, values can now be calculated for σ. Table II lists σ/a_o for various combinations of adsorbates and adsorbents with body-centered-cubic structures.

Various theories have been developed to evaluate explicitly the attractive long-range interaction energy for two dissimilar atoms. The best results seem to be obtained (ref. 4) from the theory developed by Kirkwood (ref. 15) and Müller (ref. 16). They obtained

$$E\ (\text{attractive}) = -\frac{6mc^2}{r^6}\,\frac{\alpha_A\alpha_M}{\frac{\alpha_A}{\chi_A} + \frac{\alpha_M}{\chi_M}} \tag{B1}$$

where α is the electronic polarizability, χ is the diamagnetic susceptibility, m is the electron rest mass, c is the speed of light in vacuum, the subscript A refers to the adsorbed atom, and the subscript M refers to the substrate metal atoms.

Comparison of equation (B1) with the attractive term in the Lennard-Jones potential allows evaluation of ϵ from

$$4\epsilon\sigma^6 = 6mc^2\,\frac{\alpha_A\alpha_M}{\frac{\alpha_A}{\chi_A} + \frac{\alpha_M}{\chi_M}} \tag{B2}$$

REFERENCES

1. Ehrlich, Gert: Adsorption and Surface Structure. Metal Surfaces: Structure, Energetics and Kinetics. Am. Soc. for Metals, 1963, pp. 221-286.

2. Green, Mino; and Seiwatz, Ruth: Interaction of Rare Gases With Semiconductor Surfaces. J. Chem. Phys., vol. 35, no. 3, Sept. 1961, pp. 915-921.

3. Melmed, A. J.; and Gomer, R.: Field Emission from Metal Whiskers. J. Chem. Phys., vol. 30, no. 2, Feb. 1959, pp. 586-587.

4. Pierotti, R. A.; and Halsey, G. D., Jr.: The Interaction of Krypton With Metals. An Appraisal of Several Interaction Theories. J. Phys. Chem., vol. 63, no. 5, May 1959, pp. 680-686.

5. Neustadter, Harold E.; Luke, Keung P.; and Sheahan, Thomas: Low-Coverage Heat of Adsorption. II. Alkali Metal Atoms on Tungsten; Lennard-Jones Atom-Atom Interaction Theory. NASA TN D-2431, 1964.

6. Good, R. H., Jr.; and Müller, Erwin W.: Field Emission. Handbuch der Physik, Bd. 21 S. Flügge, ed., Springer-Verlag, 1956, pp. 176-231.

7. Stranski, I. N.; and Suhrmann, R.: Electron Emission from Crystalline Metal Surfaces and Its Relation to the Crystal Structure. II. Single Crystal Surfaces with Adsorbed Impurity Atoms. Ann. Phys., Lpz. (Folge 6), vol. 1, nos. 4-5, May 1947, pp. 169-180.

8. Utsugi, H.; and Gomer, R.: Field Desorption of Barium from Tungsten. J. Chem. Phys., vol. 37, no. 8, Oct. 1962, pp. 1706-1719.

9. Drechsler, Michael: Preferred Direction of the Surface Diffusion on Single-Crystal Faces. Z. Elektrochem., vol. 58, 1954, pp. 334-339.

10. Ehrlich, Gert; and Hudda, F. G.: Interaction of Rare Gases With Metal Surfaces. I. A, Kr, and Xe on Tungsten. J. Chem. Phys., vol. 30, no. 2, Feb. 1959, pp. 493-512.

11. Ehrlich, Gert: Molecular Processes at the Gas-Solid Interface. Structure and Properties of Thin Films. Proc. Int. Conf. on Structure and Properties of Thin Films, Bolton Landing, N. Y. 1959, C. A. Neugebauer, J. B. Newkirk, and D. A. Vermilyea, eds., John Wiley & Sons, Inc., 1959, pp. 423-475.

12. Hughes, F. L.; Levinstein, H.; and Kaplan R.: Surface Properties of Etched Tungsten Single Crystals. Phys. Rev., vol. 113, no. 4, Feb. 1959, pp. 1023-1028.

13. George, T. H.; and Stier, P. M.: Chemisorption of Oxygen on Ordered Tungsten Surfaces. J. Chem. Phys., vol. 37, no. 9, Nov. 1962, pp. 1935-1946.

14. Bacigalupi, Robert J.: Surface Topography of Single Crystals of Face-Centered-Cubic, Body-Centered-Cubic, Sodium Chloride, Diamond and Zinc-Blende Structures. NASA TN D-2275, 1964.

15. Kirkwood, John G.: Polarizabilities, Susceptibilities and van der Waals Forces of Atoms With Several Electrons. Physik, Z., vol. 33, 1932, pp. 57-60.

16. Muller, Alex: The van der Waals Potential and the Lattice Energy of a n-CH_2 Chain Molecule in a Paraffin Crystal. Proc. Roy. Soc. London, ser. A, vol. 154, 1936, pp. 624-639.

17. Pauling, Linus C.: The Nature of the Chemical Bond and the Structure of Molecules and Crystals; an Introduction to Modern Structural Chemistry. Third ed., Cornell Univ. Press, 1960.

TABLE I. - NORMALIZED VALUES OF HEATS OF ADSORPTION AND DIFFUSION ACTIVATION ENERGY FOR VARIOUS ADSORBATES ON BODY-CENTERED-CUBIC SUBSTRATES

Plane (body centered cubic)	σ/a_o									
	0.80		0.894		1.00		1.123		1.20	
	$\Phi/4\epsilon$	$E_d/4\epsilon$	$\Phi/4\epsilon$	$E_d/4\epsilon$	$\Phi/4\epsilon$	$E_d/4\epsilon$	$\Phi/4\epsilon$	$E_d/4\epsilon$	$\Phi/4\epsilon$	$E_d/4\epsilon$
110	1.29	0.163	1.54	0.152	1.90	0.135	2.41	0.110	2.79	0.093
100	1.581	0.586	1.732	0.514	1.991	0.449	2.401	0.382	2.719	0.343
211	1.761	0.308	2.045	0.387	2.322	0.346	2.707	0.262	3.009	0.216
210	1.84	0.45	2.02	0.28	2.39	0.18	2.97	0.12	3.35	0.10
111	1.881	0.680	1.933	0.480	2.125	0.397	2.484	0.340	2.772	0.31
310	1.84	0.56	2.10	0.41	2.34	0.31	2.78	0.17	3.04	0.07
321	1.815	0.310	2.162	0.422	2.509	0.345	3.025	0.275	3.417	0.231
411	1.930	0.920	2.221	0.925	2.466	0.783	2.802	0.640	3.071	0.510

→ 14

TABLE II. - VALUES OF σ/a_o FOR VARIOUS ADSORBATES ON BODY-CENTERED CUBIC SUBSTRATES[a]

Adsorbate	Substrate						
	Vanadium	Chromium	Iron	Tantalum	Niobium	Molybdenum	Tungsten
Neon	0.864	0.890	0.891	0.825	0.828	0.846	0.844
Argon	0.955	0.985	0.987	0.909	0.911	0.934	0.932
Krypton	0.981	1.013	1.015	0.933	0.935	0.960	0.957
Xenon	1.040	1.075	1.077	0.987	0.990	1.017	1.013
Lithium	0.849	0.874	0.875	0.812	0.813	0.832	0.830
Sodium	0.951	0.981	0.982	0.905	0.908	0.931	0.927
Potassium	1.084	1.122	1.124	1.027	1.029	1.064	1.061
Rubidium	1.227	1.162	1.164	1.063	1.066	1.096	1.092
Cesium	1.178	1.220	1.224	1.114	1.117	1.150	1.123
Thorium	0.921	0.950	0.951	0.878	0.880	0.902	0.894
Barium	1.045	1.080	1.083	0.992	0.994	1.021	1.018
Strontium	1.017	1.050	1.053	0.966	0.968	0.994	0.991
Self-adsorption	0.784	0.785	0.784	0.786	0.787	0.787	0.785

[a]Based on atomic radii obtained from ref. 17, p. 403.

end.

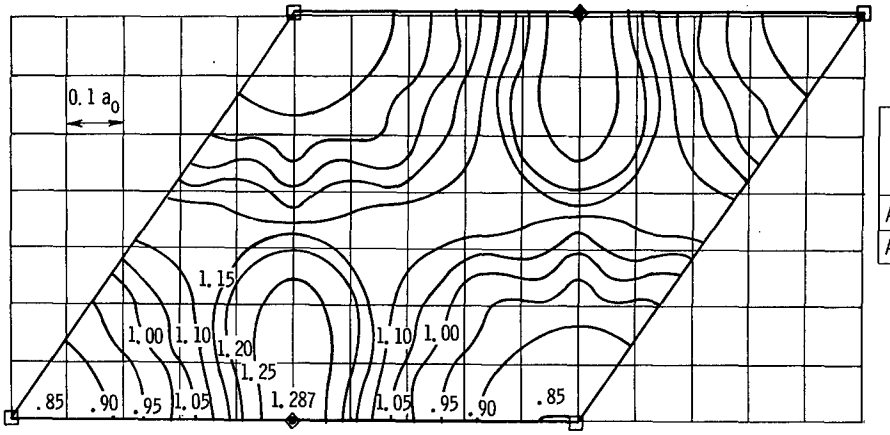

	Plane (from surface)		
	0	1	2
Atom symbol	□	◇	△
Adsorption site		●	

(a) $\sigma/a_0 = 0.80$.

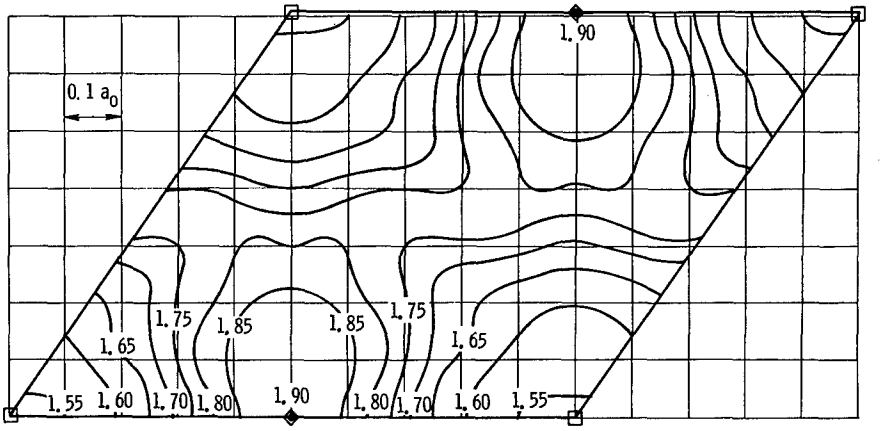

(b) $\sigma/a_0 = 1.00$.

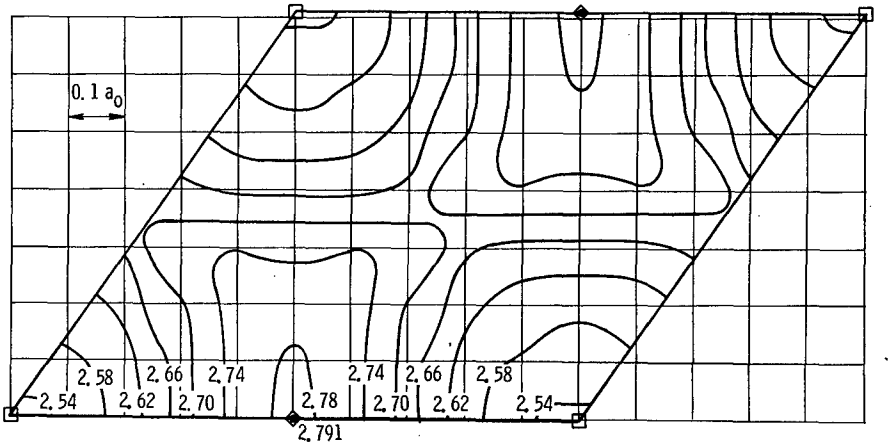

(c) $\sigma/a_0 = 1.20$.

Figure 1. - Topographical map of normalized adsorption energy on 110 plane.

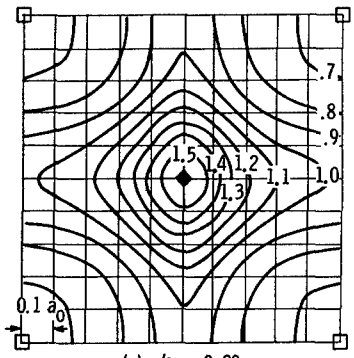

(a) $\sigma/a_0 = 0.80$.

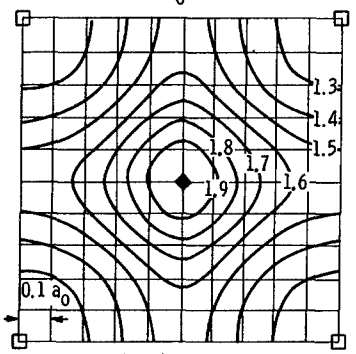

(b) $\sigma/a_0 = 1.00$.

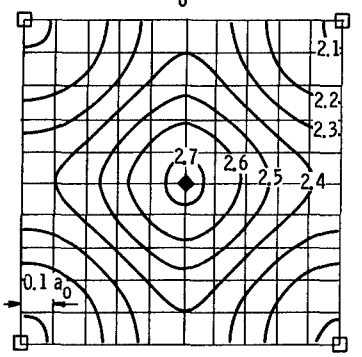

(c) $\sigma/a_0 = 1.20$.

	Plane (from surface)		
	0	1	2
Atom symbol	□	◇	△
Adsorption site		●	

Figure 2. - Topographical map of normalized adsorption energy on 100 plane.

	Plane (from surface)		
	0	1	2
Atom symbol	□	◇	△
Adsorption site	●		

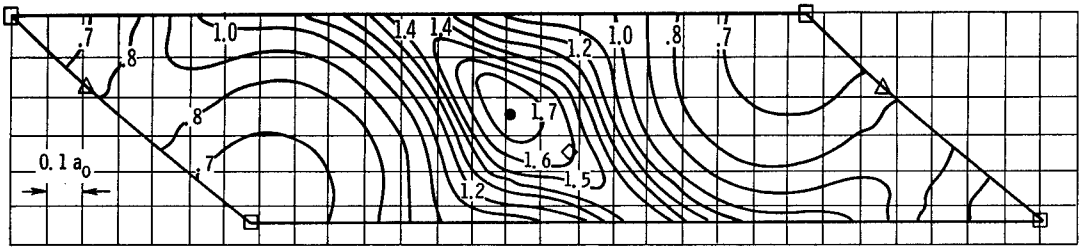

(a) $\sigma/a_0 = 0.80$.

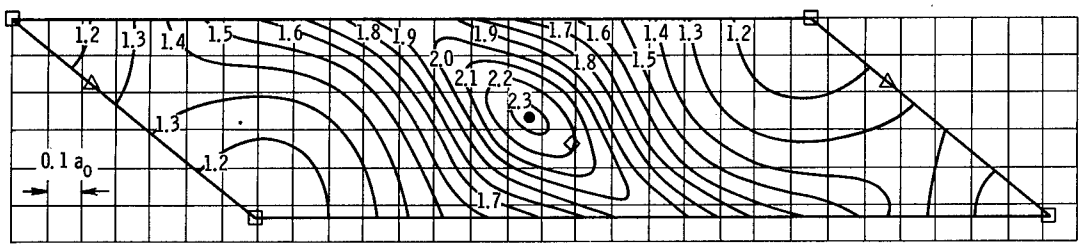

(b) $\sigma/a_0 = 1.00$.

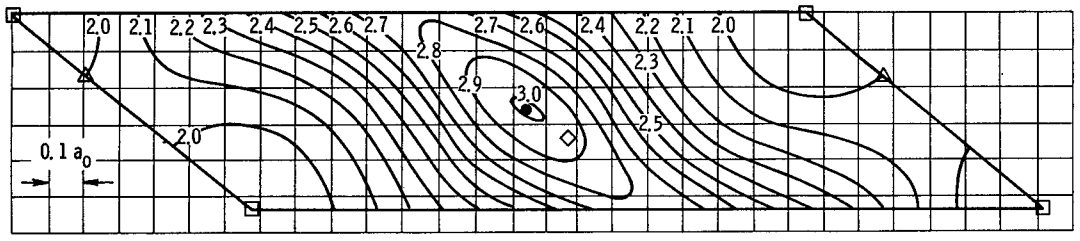

(c) $\sigma/a_0 = 1.20$.

Figure 3. - Topographical map of normalized adsorption energy on 211 plane.

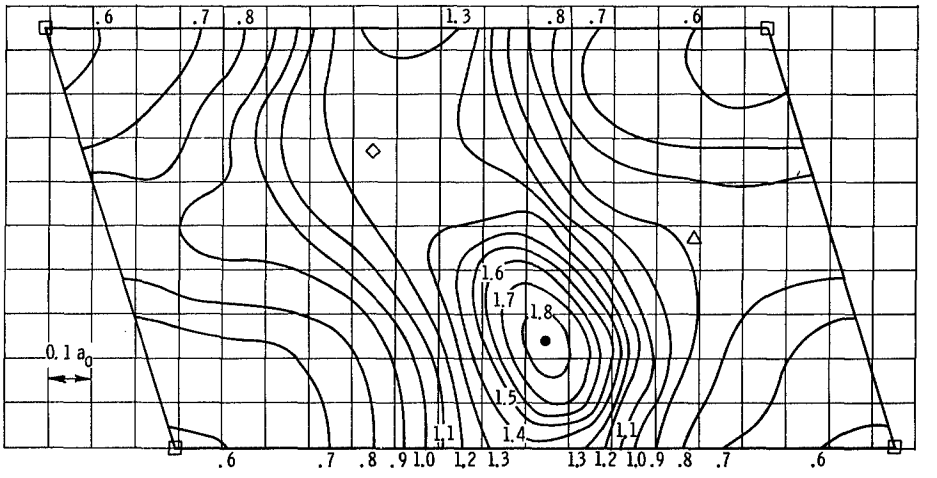

	Plane (from surface)		
	0	1	2
Atom symbol	□	◇	△
Adsorption site		●	

(a) $\sigma/a_0 = 0.80$.

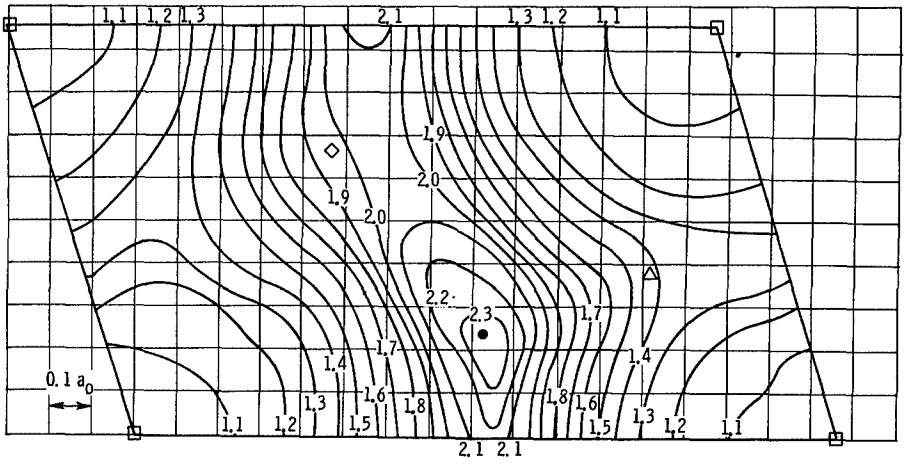

(b) $\sigma/a_0 = 1.00$.

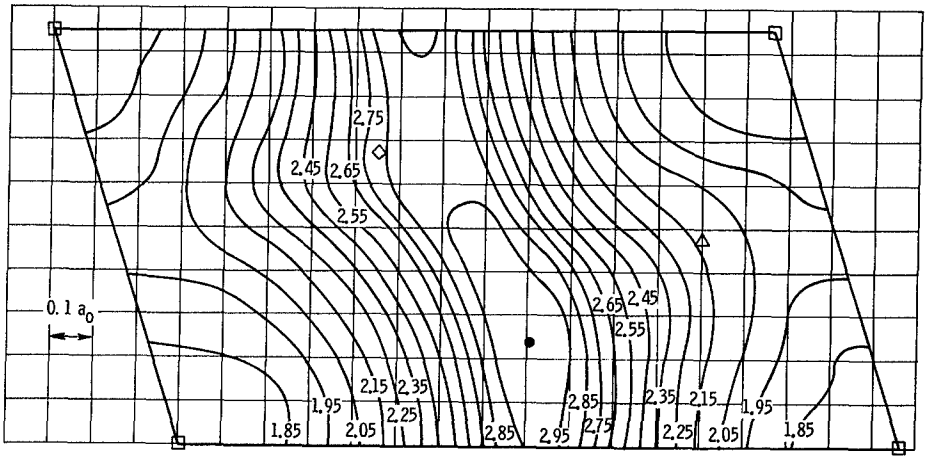

(c) $\sigma/a_0 = 1.20$.

Figure 4. - Topographical map of normalized adsorption energy on 310 plane.

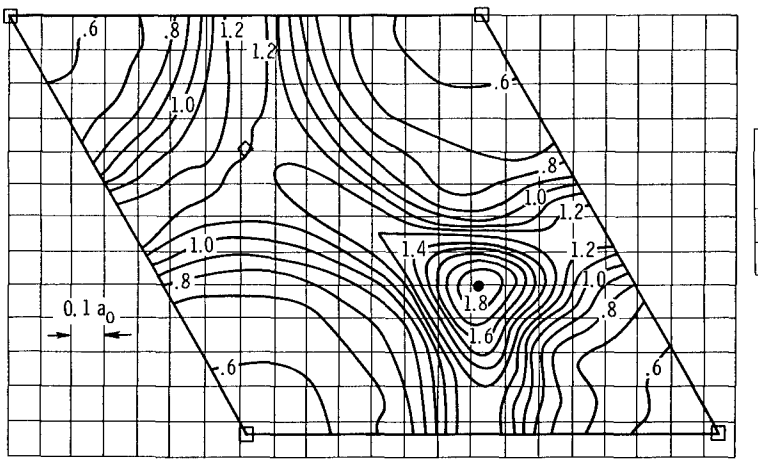

	Plane (from surface)		
	0	1	2
Atom symbol	□	◇	△
Adsorption site	●		

(a) $\sigma/a_0 = 0.80$.

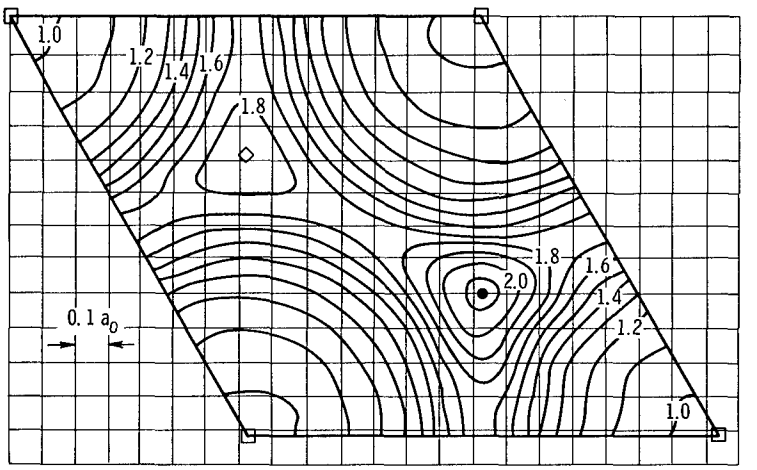

(b) $\sigma/a_0 = 1.00$.

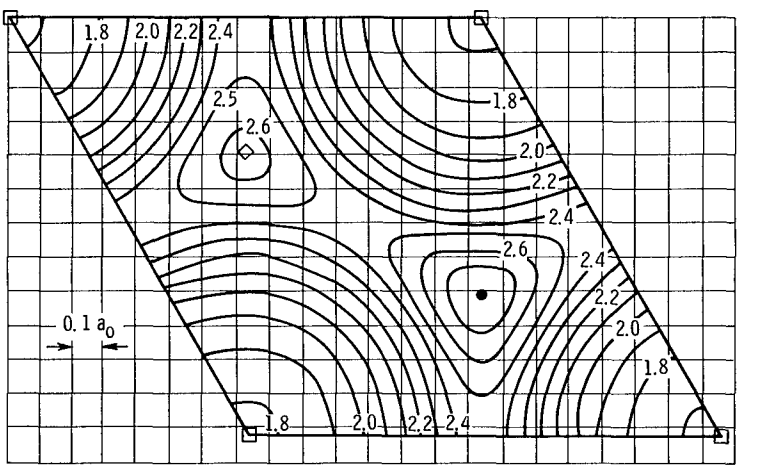

(c) $\sigma/a_0 = 1.20$.

Figure 5. - Topographical map of normalized adsorption energy on 111 plane.

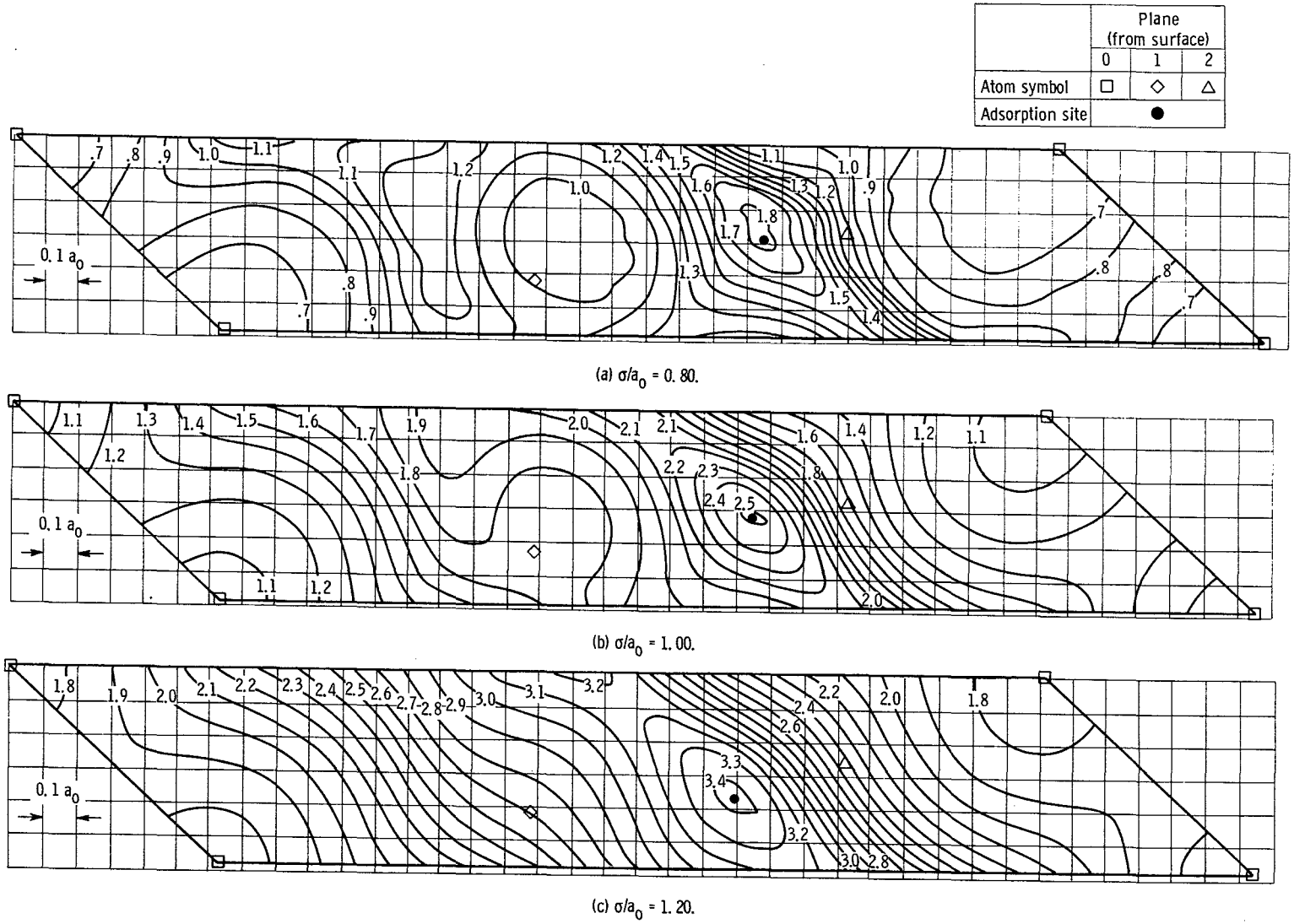

(a) $\sigma/a_0 = 0.80$.

(b) $\sigma/a_0 = 1.00$.

(c) $\sigma/a_0 = 1.20$.

Figure 6. - Topographical map of normalized adsorption energy on 321 plane.

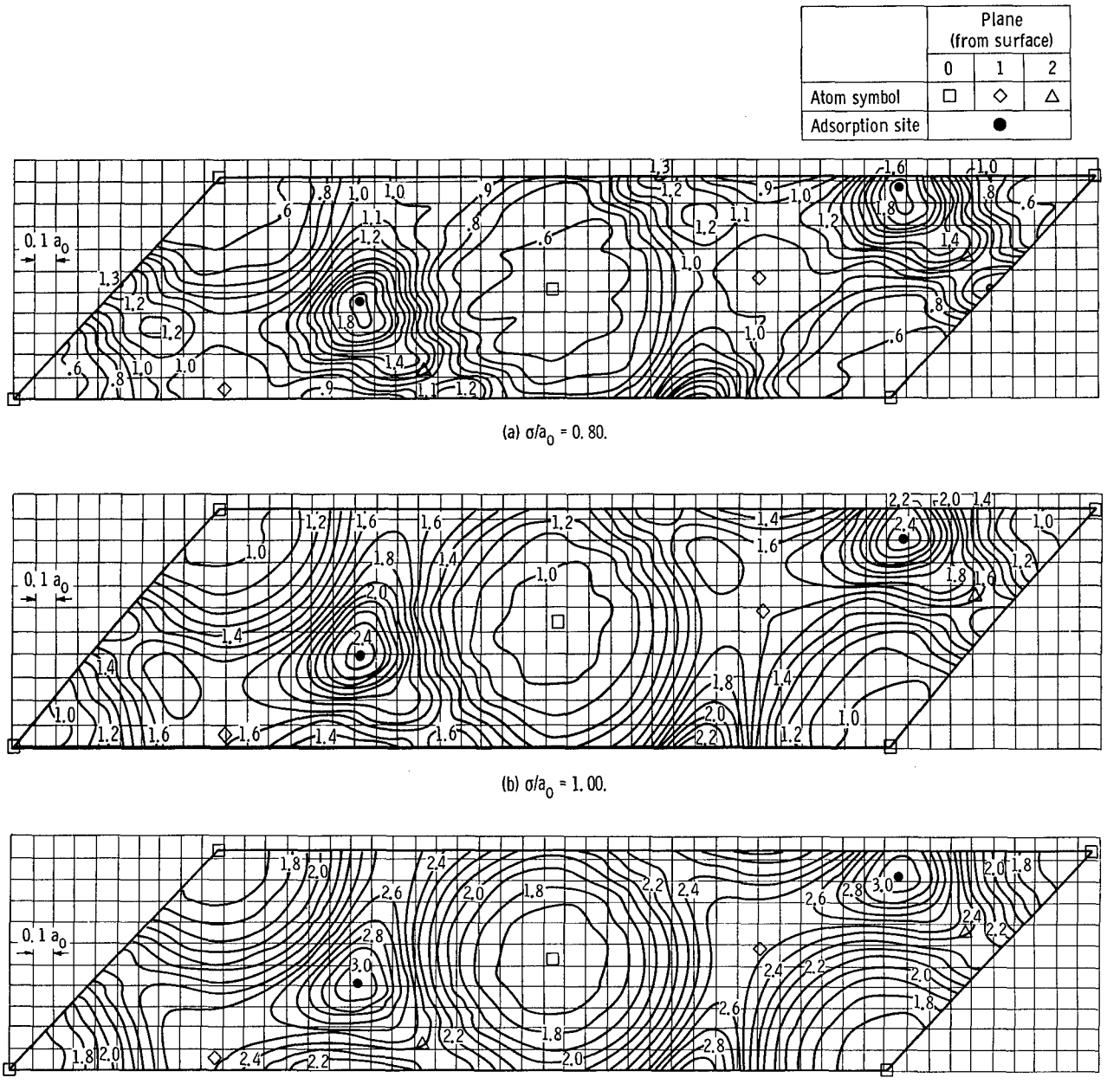

Figure 7. - Topographical map of normalized adsorption energy on 411 plane.

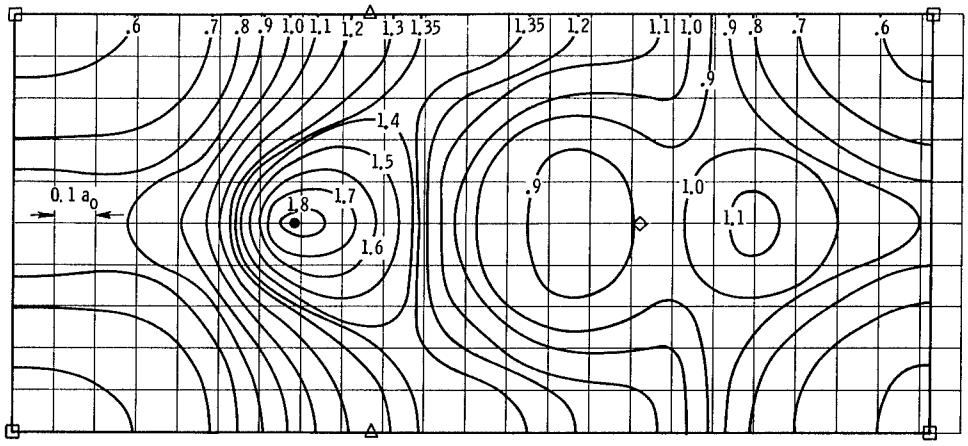

	Plane (from surface)		
	0	1	2
Atom symbol	□	◇	△
Adsorption site		●	

(a) $\sigma/a_0 = 0.80$.

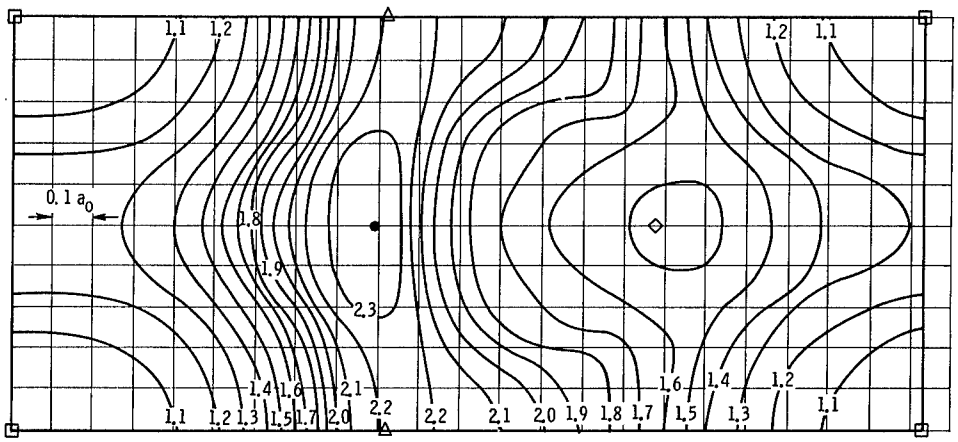

(b) $\sigma/a_0 = 1.00$.

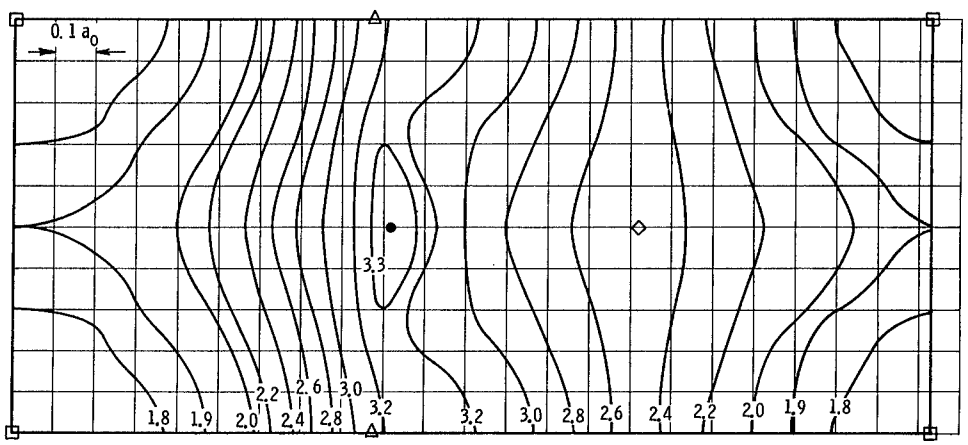

(c) $\sigma/a_0 = 1.20$.

Figure 8. - Topographical map of normalized adsorption energy on 210 plane.